CHINESE OPTICS LETTERS

Vol. 23, No. 1 | January 2025

Photonics-assisted intensity-modulation and direct-detection MIMO millimeter-wave system in the D-band

Jingwen Tan (谭景文)[1], Peng Tian (田 鹏)[1], Jianjun Yu (余建军)[1*], Xianming Zhao (赵先明)[2], Xinglin Dou (窦兴林)[2], Long Zhang (张 龙)[1], Xiongwei Yang (杨雄伟)[1], Yang Han (韩 扬)[1], Yi Wei (魏 怡)[1], Bing Zhang (张 冰)[1], Qinyi Zhang (张沁旖)[1], Luhan Jiang (姜璐涵)[1], Weiping Li (李韦萍)[1], Rahim Uddin[1], Kaihui Wang (王凯辉)[1], and Wen Zhou (周 雯)[1]

[1] State Key Laboratory of ASIC and System, Key Laboratory for Information Science of Electromagnetic Waves (MoE), School of Information Science and Technology, Fudan University, Shanghai 200433, China

[2] Beijing Hongshan Information Technology Research Institute Co., Ltd., Beijing 100176, China

*Corresponding author: jianjun@fudan.edu.cn

Received February 26, 2024 | Accepted July 9, 2024 | Posted Online January 22, 2025

We experimentally demonstrate the transmission of discrete multi-tone (DMT) millimeter-wave (mm-wave) signals over a 1.2-km distance at the D-band (110–170 GHz) in a cost-effective intensity-modulation and direct-detection (IM/DD) communication system. In the experiment, we successfully achieve the transmission of DMT-QPSK and DMT-16QAM mm-wave signals over multiple-input multiple-output (MIMO) links. After the 1.2-km free-space transmission, the bit error rate (BER) of the DMT-16QAM is below the 25% soft decision forward error correction (25% SD-FEC) threshold of 4×10^{-2}, with a maximum net bit rate of 24.62 Gbit/s achieved in this system.

Keywords: D-band; discrete multi-tone; intensity modulation and direct detection; long-distance wireless transmission; photonics-assisted technique.

DOI: 10.3788/COL202523.010601

1. Introduction

With the continuous improvement of digital infrastructure and the rapid advancement of new-generation digital technologies, such as Internet of Things (IoT), cloud computing, and artificial intelligence (AI), network data traffic has exploded, thereby posing severe challenges for current communication systems in terms of increasing transmission rates and capacity[1–3]. In order to meet the growing demand for transmission capacity and provide sufficient frequency resources, the D-band (110–170 GHz) has a larger available bandwidth to accommodate wideband signals and is an excellent choice. Photonics-assisted millimeter-wave generation technology can overcome the bandwidth limitations of electronic devices in all-electronic technology through a simple structure, making it well-suited for application in radio-over-fiber (ROF) systems[4–10]. In recent years, some representative studies on D-band wireless transmission using a photonics-assisted technique have been reported. Zhou *et al.* demonstrated the transmission of a 60 Gbit/s 8-ary pulse amplitude modulation (PAM-8) signal at 135 GHz over a 3-m wireless link.[10] Li *et al.* transmitted a 23.1 Gbit/s probabilistic shaping 64-ary quadrature amplitude modulation (PS-64QAM) signal over a 10 km optic-fiber and 4.6 km wireless distance at 135 GHz.[11] In addition, the application of multiple-input multiple-output (MIMO) technology can effectively double the transmission capacity of wireless communication systems. A 184 Gbit/s polarization-division-multiplexing quadrature phase shift keying (PDM-QPSK) signal was successfully transmitted over an 80 km single-mode fiber-28 (SMF-28) and 0.6-m 2×2 MIMO wireless link in the D-band[12]. Li *et al.* reported the transmission of a 1 Tb/s PS-64QAM signal over a 3.1-m 4×4 MIMO wireless link in the D-band.[6]

To further enhance the overall capacity and distance of wireless transmission, multi-carrier modulation techniques with high spectral efficiency and tolerance for inter-symbol interference (ISI), such as orthogonal frequency division multiplexing (OFDM) and discrete multi-tone (DMT), are widely used[13–15]. However, existing D-band wireless communication systems are mostly based on expensive and complex coherent schemes. Compared to the coherent solution, using an intensity-modulation and direct-detection (IM/DD) approach with envelope detectors (EDs) for direct detection can avoid the use of high-cost equipment, such as mixers and high-frequency local oscillators, and simplify the digital signal processing (DSP) process at the receiver, thereby reducing system costs and decreasing complexity. Envelope detection in the

millimeter-wave (mm-wave) band has been demonstrated in previous studies[16–21]. Moreover, due to the real-valued nature of DMT signals, they are well-suited for application in IM/DD systems, and many low-cost, high-capacity schemes based on IM/DD that use DMT have been proposed[15,22–24]. Therefore, transmitting DMT signals in IM/DD systems that combine a photonics-assisted technique with MIMO technology is a promising transmission solution that is expected to meet future broadband mobile communication demands.

In this paper, we propose and build a low-cost and long-distance IM/DD wireless mm-wave signal transmission system based on photonics-assisted technique. We experimentally demonstrate that the system transmits 15-GBaud DMT-QPSK and 10-GBaud DMT-16QAM mm-wave signals over MIMO links at 125 GHz, respectively. Based on the experimental results, the bit error rate (BER) of the DMT-16QAM after 1.2 km transmission is 3.44×10^{-2}, which is below the soft decision forward error correction (SD-FEC) threshold of 4×10^{-2}. Considering the SD-FEC threshold of 4×10^{-2} with 25% overhead, the system can achieve a maximum net bit rate of 24.62 Gbit/s.

2. Principles

Figure 1 shows two transmission schemes for an IM/DD MIMO wireless mm-wave signal transmission system. The mm-wave signal after intensity modulation contains a direct current (DC) component. When the transmitting and receiving antennas are in the same polarization direction, the signal at the receiver is prone to constructive and destructive interference, as shown in Fig. 1(a). Constructive interference enhances the intensity of the received signal. When the signal intensity is too high, it will cause the signal to exceed the linear working range of the photodetector, thereby causing distortion. Destructive interference leads to a reduction in signal intensity and can even result in information loss. Moreover, even if the received signal can be recovered, a more complex DSP algorithm is required, yet the quality of the received signal cannot be guaranteed.

To improve system performance, we alter the polarization direction of the transmitting and receiving antennas, utilizing polarization multiplexing to transmit signals separately in horizontal and vertical polarization directions, as shown in Fig. 1(b). Signals with different polarization directions will not interact in the same way at the receiver, effectively preventing constructive and destructive interference and ensuring high-quality signal transmission. Furthermore, due to the fact that the IM/DD system does not rely on phase information, it is well-suited for polarization multiplexing schemes without significantly increasing system complexity and cost. In addition, polarization multiplexing can increase channel capacity and enhance the spectral efficiency of the system.

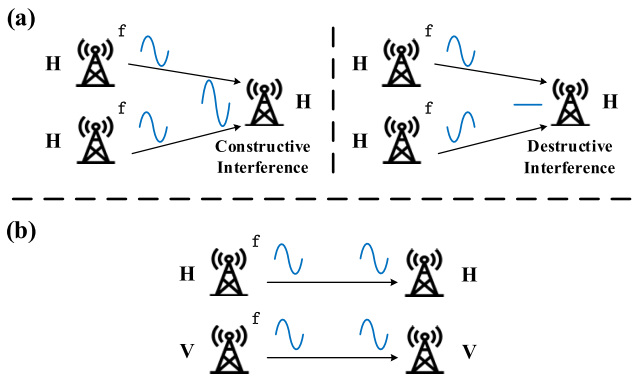

Fig. 1. Two transmission schemes for the IM/DD MIMO communication system. (a) Transmission scheme without polarization multiplexing. (b) Transmission scheme with polarization multiplexing.

3. Experimental Setup

Figure 2 shows the experimental setup for long-distance photonics-assisted D-band MIMO wireless transmission. The transmitter is located on the top floor of the Guanghua building on the Handan campus of Fudan University, and the receiver is on the roof of a residential building 1.2 km away. Photos of the transmitter, transmission link, and receiver are shown in Figs. 2(a)–2(c). Figure 2(d) shows the DMT scheme for signal generation in this experiment, known as the TX DSP. A pseudo-random binary sequence (PRBS) is generated and then mapped into QAM format. After the serial-to-parallel conversion, the discrete Fourier transform-spread (DFT-S) technique is used to suppress the peak-to-average power ratio (PAPR) of the DMT signal. We use N subcarriers loaded with data to perform an additional N-point DFT and generate 4 pilots for insertion into these data subcarriers to estimate the channel. Additionally, other N subcarriers carry Hermitian symmetric data to ensure a real signal output following a 1024-point inverse fast Fourier transform (IFFT) operation. A 16-point cyclic prefix (CP) is added to reduce the inter-symbol interference (ISI) before the parallel to serial conversion. The generated baseband DMT signal is then uploaded into an arbitrary waveform generator (AWG) with a 120 GSa/s sampling rate, and it is amplified by an electrical amplifier (EA) to drive the optical modulator. Notably, in this experiment, we set the number of data subcarriers to $N = 400$ and set other subcarriers to null to reduce high-frequency fading.

At the Tx side, two external cavity lasers (ECLs) with a linewidth of less than 100 kHz are used to generate continuous-wavelength light waves, working at 1550 and 1551 nm, respectively. The two laser beams are combined using a polarization-maintaining optical coupler (PM-OC) and then modulated by the baseband electrical DMT signal in an intensity modulator (IM). Subsequently, the modulated optical signal is amplified by a polarization-maintaining erbium-doped fiber amplifier (PM-EDFA), and an attenuator (ATT) is used to adjust the input optical power into the uni-traveling-carrier photodiode (UTC-PD). To realize 2×2 MIMO wireless transmission, the optical signal is divided into two channels by a PM-OC for separate transmission. In order to decorrelate the optical signals, one arm of the PM-OC is made 10 m longer than the other one. Both optical signals are then beaten by UTC-PDs, generating

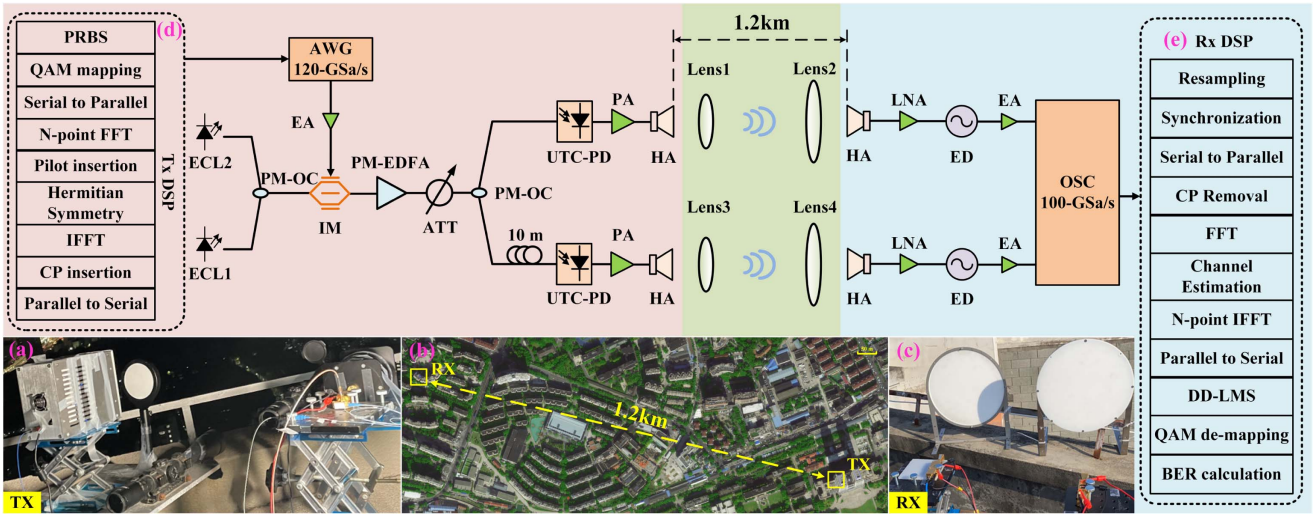

Fig. 2. Experimental setup of photonics-assisted D-band MIMO wireless communication system. Photos of (a) transmitter, (b) transmission link, and (c) receiver. (d) Tx DSP block diagram. (e) Rx DSP block diagram.

125 GHz D-band signals[12]. Then, the generated electrical signals are amplified by power amplifiers (PAs) with a saturated output power of 13 dBm. The D-band signals are radiated into free space by D-band horn antennas (HAs) with a gain of 25 dBi, oriented in horizontal and vertical polarization directions. In the wireless link, two pairs of PTFE lenses are deployed for the signal beam aggregation to support a 1.2-km wireless transmission link. Specifically, Lens 1 and Lens 3, each featuring a 10 cm diameter and a 20 cm focal length, are paired with Lens 2 and Lens 4, each with a 30 cm diameter and a 50 cm focal length.

At the Rx side, two D-band HAs are used to simultaneously receive the H- and V-polarization electrical signals. The isolation between H- and V-polarization is 25 dB. The two polarization direction signals are amplified by two low-noise amplifiers (LNAs, 110–170 GHz) with a gain of 33 dB and then down-converted to baseband DMT signals through the EDs. The signals are amplified by a pair of EAs with a gain of 26 dB and then captured by an oscilloscope (OSC) with a sampling rate of 100 GSa/s and 33 GHz electrical bandwidth for offline digital signal processing.

Figure 3(a) shows the spectrum of the baseband DMT-16QAM signal captured by the OSC when the optical power into the UTC-PD is 5 dBm. It can be seen that there are sideband tones in the spectrum caused by the clock leakage of the oscilloscope. Fortunately, these tones do not negatively impact the quality of the DMT signal transmission because the spectrum of the baseband DMT signal after resampling clearly shows an absence of harmonic components within the band, as shown in Fig. 3(b). The offline DSP routine at the receiver is shown in Fig. 2(e). The Rx DSP includes synchronization, CP removal, 1024-point fast Fourier transform (FFT), channel estimation with an intra-symbol frequency averaging (ISFA) algorithm, N-point IFFT, decision-directed least-mean square (DD-LMS), QAM de-mapping, and BER calculation[25–31].

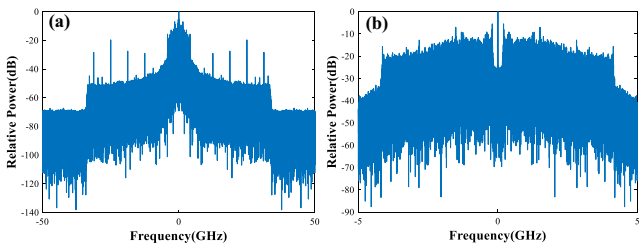

Fig. 3. (a) Baseband signal spectrum captured by OSC. (b) Baseband signal spectrum after resampling.

The experiment was conducted outdoors under favorable weather conditions. For this experiment, the wireless link power budget of the communication system was computed, as characterized by the Friis formula[32],

$$P_R = P_T + G_T + G_R - 20\log\frac{4\pi df}{c} - L_m, \tag{1}$$

where P_T represents the transmit power, G_T denotes the gain of the transmitting antenna, G_R is the gain of the receiving antenna, d, f, and c represent the wireless transmission distance, the frequency of the mm-wave signals, and the speed of light in a vacuum, respectively, and L_m denotes the atmospheric loss.

In our experiment, the output power of PA (P_T) is 13 dBm. The combined gain of the transmitting antenna and Lens 1 (G_T) is about 34 dBi, and the combined gain of the receiving antenna and Lens 2 (G_R) is about 41 dBi. Because the wireless transmission distance (d) is 1.2 km and the frequency of the mm-wave signal (f) is 125 GHz, the free space path loss $20\log\frac{4\pi df}{c}$ equals approximately 135.96 dB. On a sunny day, the atmospheric loss (L_m) is about 0.96 dB at 125 GHz for a 1.2 km wireless distance link[33]. After calculation, the received power (P_R) is approximately −48.92 dBm, which is within a 2 dB difference from

our experimental measurements. Considering other factors such as connector losses between the devices, the calculation of the received power is realistic.

4. Experimental Results and Discussion

We demonstrate the experimental results of the transmission of the DMT-QPSK and DMT-16QAM signals. To adapt to the channel environment, we used 4 pilots for channel estimation based on the zero-forcing algorithm. For improved accuracy, the ISFA algorithm is applied to smooth the estimated channel response, thereby enhancing channel estimation and equalization. To further improve the quality of the signal after channel estimation, the DD-LMS algorithm causes the constellation of the recovered QAM signal to converge near the standard QAM constellation, minimizing the error relative to these standard points. Figure 4(a) illustrates the estimated signal to noise ratio (SNR) on each subcarrier of the DMT-QPSK signal. It can be seen that both the ISFA and DD-LMS algorithms are able to improve the SNR on each subcarrier of the DMT signal. Similarly, the DMT-16QAM signal also exhibits the same results, with the estimated SNR on each subcarrier of the DMT-16QAM signal as shown in Fig. 4(d). Figures 4(b) and 4(c), respectively, show the constellation of the QPSK recovered from the DMT signal before and after the DD-LMS. It can be clearly observed that the phase of the QPSK signal after the DD-LMS is adjusted and corrected, and the signal is well converged at the ideal constellation. Furthermore, after the application of the DD-LMS, the quality of the 16QAM signal has also been significantly improved, allowing it to converge near the ideal constellation. However, due to the higher order, there are more scatter points around the ideal constellation, as shown in Figs. 4(e) and 4(f).

Figure 5 shows the BER versus the input power into the UTC-PD for the DMT-QPSK after 1.2-km wireless transmission. It can be seen that the BER curves of the 10-GBaud and the 15-GBaud DMT-QPSK follow a generally consistent trend. As the optical power increases, the BER performance gradually improves, reaching its peak when the optical power is at 5 dBm, where both 10-GBaud and 15-GBaud signals exhibit the lowest BER. Yet the BER performance gradually deteriorates when the optical power exceeds 5 dBm due to increasing saturation in the system that affects the quality of signal transmission. For the 10-GBaud DMT-QPSK signal, the system saturation effect is minimal, and the optimal BER performance is achieved at optical powers of 4.5 and 5 dBm. The corresponding BER is 2.77×10^{-3}, which is below the hard-decision forward error correction (HD-FEC) threshold of 3.8×10^{-3}, and the recovered QPSK constellation is shown in Fig. 5(a). With increasing rates, the signal's BER performance degrades. The BER for the 15-GBaud DMT-QPSK signal basically remains within the 20% SD-FEC threshold of 2×10^{-2}. At the point of best BER performance, the recovered QPSK constellation is illustrated in Fig. 5(b).

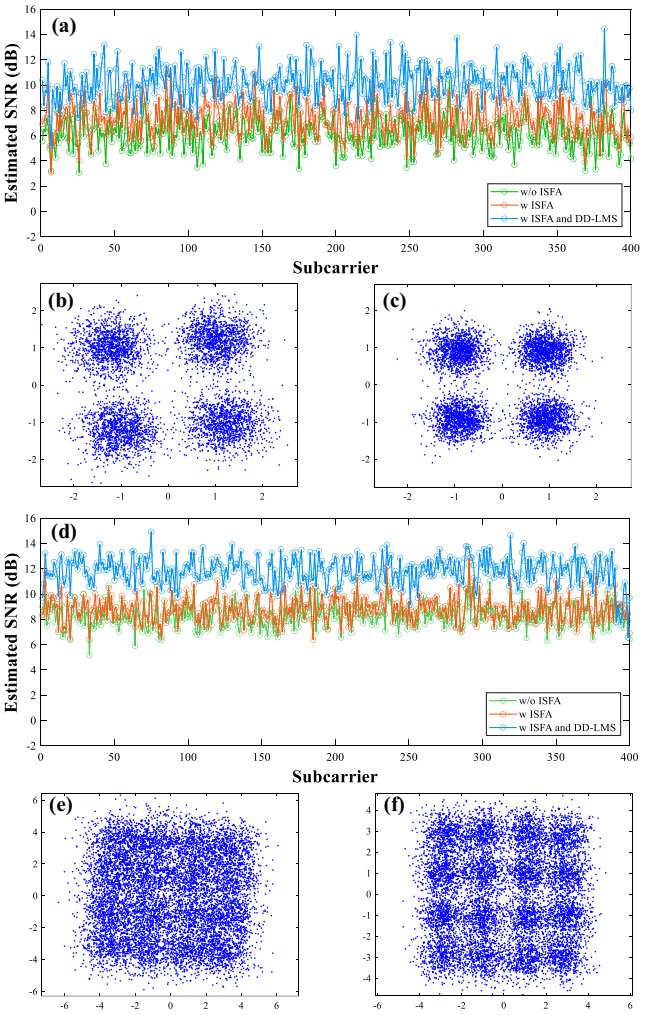

Fig. 4. (a) Estimated SNR on each subcarrier of the DMT-QPSK signal. (b) Constellation of the recovered QPSK before DD-LMS. (c) Constellation of the recovered QPSK after DD-LMS. (d) Estimated SNR on each subcarrier of the DMT-16QAM signal. (e) Constellation of the recovered 16QAM before DD-LMS. (f) Constellation of recovered 16QAM after DD-LMS.

Figure 6 shows the BER of the 10-GBaud DMT-16QAM versus different input optical powers into the UTC-PD after 1.2 km wireless transmission. At the 25% SD-FEC threshold of 4×10^{-2}, the required optical power for the 10-GBaud DMT-16QAM signal transmission is 5 dBm and the minimum BER is 3.44×10^{-2}. The inset in Fig. 6 shows the constellation of the recovered 16QAM at 5 dBm optical power. Due to the impact of system saturation, the signal quality is significantly degraded. At an optical power of 5.5 dBm, the BER exceeds the 25% SD-FEC threshold. The saturation effect is evident in the time-domain waveform of the received signal, as shown in Fig. 7. It can be observed that when the optical power is at 5 dBm, the time-domain waveform is essentially symmetrical, with no apparent distortion. However, at an optical power of 5.5 dBm, the waveform is no longer symmetrical and exhibits noticeable flattening at the top, resulting in degraded signal

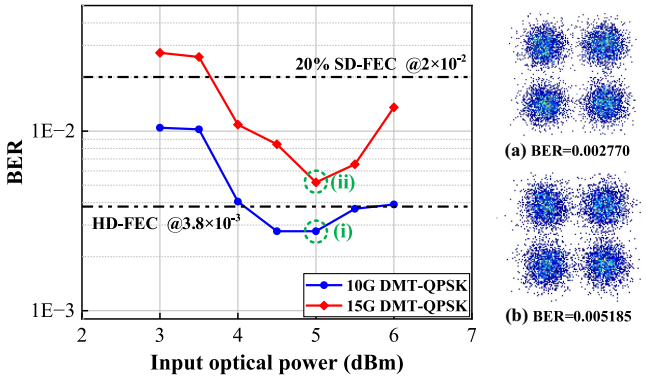

Fig. 5. Measured BER of the DMT-QPSK versus different input optical powers into UTC-PD. (a) Constellation of the QPSK recovered from the 10-GBaud DMT signal at 5-dBm input optical power into UTC-PD. (b) Constellation of the QPSK recovered from the 15-GBaud DMT signal at 5-dBm input optical power into UTC-PD.

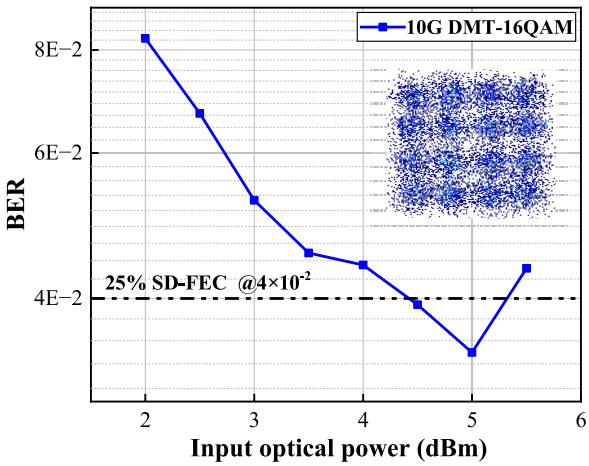

Fig. 6. Measured BER of the DMT-16QAM versus different input optical powers into the UTC-PD.

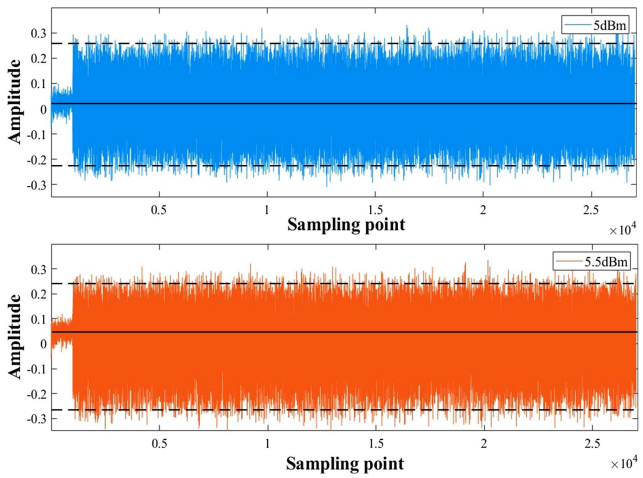

Fig. 7. Waveforms of the DMT-16QAM signals when the input optical powers into the UTC-PD are 5 and 5.5 dBm.

quality and reduced bit error performance. For this photonics-assisted D-band IM/DD MIMO wireless communication system, the DMT-16QAM net bit rate after 25% FEC overhead is removed is $10\times2\times\log2(16)\times400/(1024+16)/(1+25\%)=24.62\,\text{Gbit/s}$.

5. Conclusion

In this paper, 10-GBaud (24.62-Gbit/s) DMT-16QAM mm-wave signal MIMO wireless transmission over a 1.2 km distance at the D-band has been experimentally demonstrated in a low-cost photonics-assisted IM/DD communication system. Thanks to the ISFA and DD-LMS algorithms, the SNR on each subcarrier is effectively enhanced, thereby improving the quality of the signal transmission. In such a system, 15-GBaud DMT-QPSK and 10-GBaud DMT-16QAM signals are successfully achieved with a BER below the SD-FEC thresholds of 2×10^{-2} and 4×10^{-2} after 1.2-km long-distance wireless transmission, respectively. The experimental results demonstrate that our photonics-assisted IM/DD MIMO wireless communication system provides a low-cost and promising solution for long-distance wireless transmission in the future.

Acknowledgements

This work was supported by the National Key R&D Program of China (No. 2023YFB2905600), the National Natural Science Foundation of China (Nos. 61935005, 62127802, 62331004, and 62305067), and the Key Project of Jiangsu Province of China (No. BE2023001-4).

References

1. M. Agiwal, A. Roy, and N. Saxena, "Next generation 5G wireless networks: a comprehensive survey," IEEE Commun. Surv. Tutorials **18**, 1617 (2016).
2. W. Li, J. Yu, B. Zhu, *et al.*, "Photonics 60 GBaud PDM-16QAM fiber-wireless 2 × 2 MIMO delivery at THz-band," Chin. Opt. Lett. **21**, 073901 (2023).
3. Y. Wang, K. Wang, W. Zhou, *et al.*, "Photonic aided vector millimeter-wave signal generation without digital-to-analog converter," Chin. Opt. Lett. **19**, 011101 (2021).
4. L. Zhao, K. Wang, and W. Zhou, "Transmission of 4096-QAM OFDM at D-band," Opt. Express **31**, 2270 (2023).
5. F. Wang, J. Yu, Y. Wang, *et al.*, "Delivery of polarization-division-multiplexing wireless millimeter-wave signal over 4.6-km at W-band," J. Lightwave Technol. **40**, 6339 (2022).
6. X. Li, J. Yu, L. Zhao, *et al.*, "1-Tb/s Millimeter-wave signal wireless delivery at D-band," J. Lightwave Technol. **37**, 196 (2019).
7. Y. Cai, X. Gao, Y. Ling, *et al.*, "Power-efficient heterodyne radio over fiber link with laser phase noise robustness," Chin. Opt. Lett. **17**, 110602 (2019).
8. Q. Xu, Q. Ye, Z. Pan, *et al.*, "Generation of millimeter-wave sub-carrier optical pulse by using cascaded all-pass cavities," Chin. Opt. Lett. **8**, 7 (2010).
9. X. Yang, J. Yu, X. Zhao, *et al.*, "41.7-Gb/s D-band signals wireless delivery over 4.6 km distance based on photonics-aided technology," Opt. Laser Technol. **174**, 110660 (2024).
10. W. Zhou, L. Zhao, J. Zhang, *et al.*, "135-GHz D-band 60-Gbps PAM-8 wireless transmission employing a joint DNN equalizer with BP and CMMA," J. Lightwave Technol. **38**, 3592 (2020).
11. W. Li, J. Yu, J. Ding, *et al.*, "23.1-Gb/s 135-GHz wireless transmission over 4.6-Km and effect of rain attenuation," IEEE Trans. Microwave Theory Techn. **71**, 5004 (2023).

12. X. Li and J. Yu, "Over 100 Gb/s ultrabroadband MIMO wireless signal delivery system at the D-band," IEEE Photonics J. **8**, 1 (2016).
13. W. H. Gunawan, C.-W. Chow, Y. Liu, *et al.*, "Embedded Orthogonal-Frequency-Division-Multiplexing (OFDM) to Color-Shift-Keying (CSK) Modulation for Laser-Diode based Visible Light Communication (VLC)," in *Optical Fiber Communication Conference (OFC) 2021* (Optica Publishing Group, 2021), p. F1A.3.
14. J. Ding, J. Zhang, and J. Yu, "Comparison of geometrically shaped and probabilistically shaped bit-loading DMT for optical interconnect system," IEEE Photonics J. **12**, 1 (2020).
15. J. Ding, J. Zhang, Y. Wei, *et al.*, "Comparison of geometrically shaped 32-QAM and probabilistically shaped 32-QAM in a bandwidth-limited IM-DD System," J. Lightwave Technol. **38**, 4352 (2020).
16. C. Liu, S.-H. Fan, L. Zhang, *et al.*, "Duobinary RF envelope detection in coherent optical millimeter-wave systems," in *2012 IEEE Photonics Society Summer Topical Meeting Series* (IEEE, 2012), p. 157.
17. C. Liu, A. Yi, M. Zhu, *et al.*, "A novel direct-modulation envelope-detection Pol-Mux MIMO RoF system based on blind equalization techniques," in *Optical Fiber Communication Conference/National Fiber Optic Engineers Conference* (Optica Publishing Group, 2013), p. OM3D.6.
18. M. Chen, J. Yu, and X. Xiao, "Real-time Q-band OFDM-RoF systems with optical heterodyning and envelope detection for downlink transmission," IEEE Photonics J. **9**, 1 (2017).
19. D. Guo, Q. Zhang, X. Xin, *et al.*, "Adaptive Reed–Solomon coding and envelope detection of photonic vector signal in V-band radio over fiber system," Opt. Commun **439**, 210 (2019).
20. L. Zhang, K. Wang, Z. Zhu, *et al.*, "Real-time demonstration of photonics-assisted W-band 23 Gbps PS-64QAM DMT signals over 40.5-m wireless based on FPGA," in *Optical Fiber Communication Conference (OFC)* (Optica Publishing Group, 2024), p. Th4B.3.
21. X. Yang, W. Zhou, X. Zhao, *et al.*, "32-Gb/s CAP signals wireless delivery at D-band over 4.6 Km based on photonics-aided technology and envelope detection," J. Lightwave Technol. **42**, 4809 (2024).
22. Y. Wei, C. Liu, B. Sang, *et al.*, "Demonstration of 200 Gbit/s single λ dual band DMT transmission with a SE of 6.29 bit/s/Hz," J. Lightwave Technol. **39**, 2754 (2021).
23. L. Zhang, K. Wang, C. Wang, *et al.*, "Real-time demonstration of a low-complexity PS scheme for 16QAM-DMT signals in an IM-DD system," Opt. Express **31**, 11447 (2023).
24. L. Zhang, K. Wang, C. Wang, *et al.*, "Demonstration of real-time DMT-WDM-PON employing probabilistic shaping based on intra-symbol bit-weighted distribution matching," J. Lightwave Technol. **42**, 532 (2023).
25. J. Zhang, J. Yu, Z. Jia, *et al.*, "400 G transmission of Super-Nyquist-filtered signal based on single-carrier 110-GBaud PDM QPSK with 100-GHz grid," J. Lightwave Technol. **32**, 3239 (2014).
26. J. Yu, "1.2 Tbit/s orthogonal PDM-RZ-QPSK DWDM signal transmission over 1040 km SMF-28," Electron. Lett. **46**, 775 (2010).
27. J. Yu, Z. Dong, and N. Chi, "1.96 Tb/s (21 × 100 Gb/s) OFDM optical signal generation and transmission over 3200-km fiber," IEEE Photon. Technol. Lett. **23**, 1061 (2011).
28. J. Yu, Z. Dong, J. Zhang, *et al.*, "Generation of coherent and frequency-locked multi-carriers using cascaded phase modulators for 10 Tb/s optical transmission system," J. Lightwave Technol. **30**, 458 (2012).
29. J. Yu and Y. Wu, "High-speed optical fiber communication in China," ACS Photonics **10**, 2128 (2023).
30. X. Zhou and J. Yu, "Multi-level, multi-dimensional coding for high-speed and high-spectral-efficiency optical transmission," J. Lightwave Technol. **27**, 3641 (2009).
31. J. Yu, M.-F. Huang, D. Qian, *et al.*, "Centralized lightwave WDM-PON employing 16-QAM intensity modulated OFDM downstream and OOK modulated upstream signals," IEEE Photon. Technol. Lett. **20**, 1545 (2008).
32. H. T. Friis, "A note on a simple transmission formula," Proc. IRE **34**, 254 (1946).
33. X. Li, J. Xiao, and J. Yu, "Long-distance wireless mm-wave signal delivery at W-band," J. Lightwave Technol. **34**, 661 (2016).